PERGAMON

Available online at www.sciencedirect.com

SCIENCE DIRECT®

Polyhedron 22 (2003) 725–733

POLYHEDRON

www.elsevier.com/locate/poly

Iron(II) complexes of (pyrazol-3-yl)pyrazine. Anion-dependent formation of a hydrogen-bonded, chiral nanoporous lattice

Robert J. Smithson [a], Colin A. Kilner [a], Adrian R. Brough [b], Malcolm A. Halcrow [a,*]

[a] *Department of Chemistry, University of Leeds, Woodhouse Lane, Leeds, LS2 9JT, UK*
[b] *School of Civil Engineering, University of Leeds, Woodhouse Lane, Leeds, LS2 9JT, UK*

Received 18 July 2002; accepted 14 August 2002

Abstract

Slow evaporation of aqueous solutions of (pyrazol-3-yl)pyrazine (L^1) and $FeCl_2$, $Fe(ClO_4)_2$ or $Fe(BF_4)_2$ yields $[FeCl_2(L^1)_2]\cdot H_2O$ (**1**·H_2O), $[Fe(L^1)_3](ClO_4)_2\cdot H_2O$ (**2**·H_2O) and $[Fe(L^1)_3](BF_4)_2\cdot 2H_2O$ (**3**·$2H_2O$). The crystal structure of **1**·H_2O shows a distorted *cis*-octahedral high-spin Fe(II) centre. Molecules of **1** associate in the crystal through hydrogen bonding into 1D chains, which are linked into a 2D lattice by O–H···Cl hydrogen bonds to the lattice water. The structures of **2**·H_2O and **3**·$2H_2O$ contain low-spin Fe(II) ions. In **2**, the complex dication has a distorted *mer*-octahedral geometry, while in **3** the complex crystallises as its *fac*-octahedral isomer, with crystallographic C_3 symmetry. The complex dications in **3**·$2H_2O$ associate through hydrogen bonding into a hexagonal, chiral honeycomb structure with pores of diameter 5.3 Å. These channels are filled with a disordered region of electron density, which must contain one BF_4^- equivalent and lattice water. Attempts to remove the water from **3**·$2H_2O$ by heating under vacuum were unsuccessful, while partial replacement of the BF_4^- ions for Cl^- in toluene results in decomposition of the crystalline sample.

Keywords: Iorn; Crystal sturcture; Nonporous solids

1. Introduction

There is continuing interest in the chemistry and physics of compounds that exhibit spin-state transitions upon cooling, irradiation and/or the application of pressure [1,2]. Since these transitions are usually accompanied by a colour change in the sample, such compounds in the solid state have potential for application in information storage and display devices [3]. In order to be useful, a thermal spin-crossover compound must exhibit an abrupt transition, which should ideally occur close to room temperature, and exhibit a hysteresis loop. That is, the transition should occur cooperatively in the solid, giving a compound that is bistable at or near room temperature [4,5].

We have recently developed an interest in this area, through the Fe(II) complexes of 2,6-di(pyrazolyl)pyridine ligands, whose spin-states can be varied controllably by appropriate substitution at the ligand framework [6–8]. In order to improve the cooperativity in spin-state transitions, it is desirable to maximise intermolecular bonding between Fe centres in the solid. With this in mind, we have begun to examine the Fe(II) chemistry of pyrazine-containing chelate ligands, which contain a built-in hydrogen-bond acceptor that could be used to mediate intermolecular interactions. We report here the syntheses and crystal structures of three Fe(II) complexes of (pyrazol-3-yl)pyrazine (L^1) [9], which is of particular interest in containing hydrogen-bond donor and acceptor sites in the same molecule. Although no complexes of L^1 have been reported before, the related compounds $[Fe(L^2)_3]X_2$ [10,11] and $[Fe(L^3R)_3]X_2$ [12,13] (R = H, Me; X^- = monovalent anion) exhibit spin-state transitions below room temperature, which depend markedly on the identity of X^- and the degree of hydration of their solids. During this work, we have serendipitously obtained a nanoporous crystalline solid formed from a hydrogen-bonded network of *fac*-

* Corresponding author. Tel.: +44-113-343-6506; fax: +44-113-343-6565.
E-mail address: m.a.halcrow@chem.leeds.ac.uk (M.A. Halcrow).

0277-5387/02/$ - see front matter © 2002 Elsevier Science Ltd. All rights reserved.
doi:10.1016/S0277-5387(02)01403-1

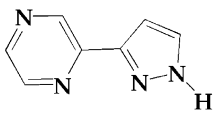

L^1

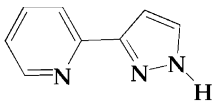

L^2

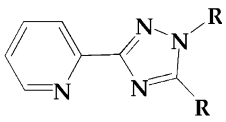

R = H, L^3H
R = Me, L^3Me

$[Fe(L^1)_3]^{2+}$ dications. Molecule-based nanoporous compounds like this are of great interest, since the potential for selective guest inclusion within their pores could lead to uses as sensors, molecular sieves or catalysts [14].

2. Experimental

All manipulations were carried out in air, using distilled water or reagent-grade solvents. L^1 was prepared by the literature procedure [9], while all Fe salts were purchased from Aldrich.

2.1. Syntheses of $[FeCl_2(L^1)_2]\cdot H_2O$ (**1**·H_2O)

Aqueous solutions of L^1 (0.50 g, 3.42×10^{-3} mol) and $FeCl_2\cdot 4H_2O$ (0.23 g, 1.14×10^{-3} mol) were mixed at room temperature. The resultant maroon solution was filtered, and allowed to evaporate slowly at ambient temperature to afford a maroon powder. Yield of crude product 0.31 g, 62%. Small amounts of this compound can be extracted into MeOH, in which it is sparingly soluble. Vapour diffusion of Et_2O into the resultant red–orange solution gave maroon crystals of the product. *Anal*. Found: C, 38.8; H, 3.3; N, 25.6; Cl, 16.2%. Calc. for $C_{14}H_{12}Cl_2FeN_8\cdot H_2O$: C, 38.5; H, 3.2; N, 25.6; Cl, 16.2%. Fast atom bombardment (FAB) mass spectrum: *m/z* 509 $[^{56}Fe^{35}_2Cl_3(L^1)_2]^+$, 383 $[^{56}Fe^{35}Cl(L^1)_2]^+$, 347 $[^{56}Fe(L^1)_2-H]^+$, 237 $[^{56}Fe^{35}ClL^1]^+$, 146 $[L^1]^+$. IR spectrum (nujol): 3105w, 1637w, 1526m, 1504w, 1403s, 1295m, 1210m, 1172m, 1141, 1055m, 1029m, 968w, 923w, 856w, 798s, 784s, 698w cm^{-1}.

2.2. Synthesis of $[Fe(L^1)_3](ClO_4)_2\cdot H_2O$ (**2**·H_2O)

Aqueous solutions of L^1 (0.50 g, 3.42×10^{-3} mol) and $Fe(ClO_4)_2\cdot 6H_2O$ (0.41 g, 1.14×10^{-3} mol) were mixed at room temperature, yielding a maroon solution. This was filtered, and allowed to evaporate slowly at ambient temperature to give air-stable dark brown crystals of X-ray quality. Yield 0.68 g, 86%. *Anal*. Found: C, 35.4; H, 2.9; N, 23.7; Cl, 10.0%. Calc. for $C_{21}H_{18}Cl_2FeN_{12}O_8\cdot H_2O$: C, 35.5; H, 2.8; N, 23.6; Cl, 10.0%. FAB mass spectrum: *m/z* 347 $[Fe(L^1)_2-H]^+$, 146 $[L^1]^+$. IR spectrum (nujol): 3542w, 3151m, 1633w, 1528m, 1409s, 1364m, 1320w, 1300w, 1211m, 1173m, 1100vs, 973w, 926m, 846m, 793s, 701w, 660w, 648m, 625s cm^{-1}. (Caution. While we have experienced no difficulty in handling **2**·H_2O, metal-organic perchlorates are potentially explosive and should be handled with due care in small quantities).

2.3. Synthesis of $[Fe(L^1)_3](BF_4)_2\cdot 2H_2O$ (**3**·$2H_2O$)

Method as for **2**·H_2O, using $Fe(BF_4)_2\cdot 6H_2O$ (0.38 g, 1.14×10^{-3} mol). The product crystallised from water as dark brown plates. Yield 0.70 g, 92%. *Anal*. Found: C, 35.9; H, 3.3; N, 23.9; F, 20.8%. Calc. for $C_{21}H_{18}B_2F_8FeN_{12}\cdot 2H_2O$: C, 35.8; H, 3.1; N, 23.9; F, 21.6%. FAB mass spectrum: *m/z* 367 $[^{56}FeF(L^1)_2]^+$, 347 $[^{56}Fe(L^1)_2-H]^+$, 146 $[L^1]^+$. IR spectrum (nujol): 3540m, 3417m, 3107w, 1634m, 1532m, 1414m, 1300w, 1225m, 1180m, 1060vs, 935m, 843w, 786m, 765m, 701w, 661m, 617w cm^{-1}. ^1H NMR spectrum (CD_3CN, 293 K): peaks from Fe-containing species; δ 17.0 (1H), 13.7 (1H), 12.5 (2H), 11.0 (1H), 10.2 (1H): peaks from uncoordinated L^1 [9]; δ 9.2 (1H), 8.5 (2H), 7.7 (1H), 6.9 (1H).

2.4. Single crystal X-ray structure determinations

Experimental details from the structure determinations are given in Table 1. All data were collected on a Nonius KappaCCD area-detector diffractometer, using graphite-monochromated Mo Kα radiation. The structures were solved by direct methods (SHELXS-97 [15]) and refined by full matrix least-squares on F^2 (SHELXL-97 [16]).

2.5. X-ray structure determination of $[FeCl_2(L^1)_2]\cdot H_2O$ (**1**·H_2O)

No disorder was detected during the refinement of this structure, and no restraints were applied. All non-H atoms were refined anisotropically, while all H atoms were located in the difference map and allowed to refine freely.

Table 1
Experimental details for the single crystal structure determinations in this study

	$[FeCl_2(L^1)_2]\cdot H_2O$ (**1**·H_2O)	$[Fe(L^1)_3](ClO_4)_2\cdot H_2O$ (**2**·H_2O)	$[Fe(L^1)_3](BF_4)_2\cdot 2H_2O$ (**3**·$2H_2O$)
Formula	$C_{14}H_{14}Cl_2FeN_8O$	$C_{21}H_{20}Cl_2FeN_{12}O_9$	$C_{21}H_{22}B_2F_8FeN_{12}O_2$
M_r	437.08	711.24	703.98
Crystal size (mm)	$0.10 \times 0.07 \times 0.02$	$0.20 \times 0.19 \times 0.13$	$0.31 \times 0.17 \times 0.11$
Crystal class,	triclinic	monoclinic	hexagonal
Space group	$P\bar{1}$	$P2_1/c$	$P3_1/c$
a (Å)	8.2948(2)	10.9878(2)	12.6485(2)
b (Å)	8.3110(2)	17.9549(4)	–
c (Å)	13.4679(4)	16.8176(3)	10.9828(1)
α (°)	86.353(1)	–	–
β (°)	84.397(1)	121.157(1)	–
γ (°)	70.964(2)	–	–
V (Å^3)	872.99(4)	2839.26(10)	1521.67(4)
Z	2	4	2
μ (Mo Kα) (mm^{-1})	1.192	0.793	0.588
T (K)	150(2)	150(2)	150(2)
Radiation λ (Å)	0.71073	0.71073	0.71073
Independent reflections	3988	6498	2302
R_{int}	0.081	0.059	0.051
Absorption correction	Multi-scan	Multi-scan	Multi-scan
Min/max transmission	0.89, 0.98	0.86, 0.90	0.84, 0.94
Observed reflections [$I > 2\sigma(I)$]	3304	5341	2248
Range in 2θ (°)	$5.9 \leqslant 2\theta \leqslant 55.0$	$4.2 \leqslant 2\theta \leqslant 55.0$	$6.4 \leqslant 2\theta \leqslant 54.9$
Range in h	$-10 \leqslant h \leqslant 10$	$-14 \leqslant h \leqslant 13$	$-16 \leqslant h \leqslant 16$
Range in k	$-10 \leqslant k \leqslant 10$	$-23 \leqslant k \leqslant 23$	$-16 \leqslant k \leqslant 16$
Range in l	$-17 \leqslant l \leqslant 17$	$-21 \leqslant l \leqslant 21$	$-13 \leqslant l \leqslant 14$
Parameters/restraints	291/0	456/32	158/1
$R(F)$ [a], $wR(F^2)$ [b]	0.036, 0.096	0.059, 0.148	0.038, 0.106
Goodness of fit	1.076	1.118	1.071
Weighting scheme [c]	$w = 1/[\sigma^2(F_o^2)+(0.0427P)^2 +0.3285P]$	$w = 1/[\sigma^2(F_o^2)+(0.0406P)^2 +6.6947P]$	$w = 1/[\sigma^2(F_o^2)+(0.0803P)^2 +0.2883P]$
$\Delta\rho$ (max/min) (e Å^{-3})	0.38/−0.68	0.71/−0.69	0.39/−0.32
Flack parameter	–	–	0.001(18)

	$[Fe(L^1)_3](BF_4)_2\cdot 2H_2O$ (**3**·$2H_2O$)
Formula	$C_{21}H_{22}B_2F_8FeN_{12}O_2$
M_r	703.98
Crystal size (mm)	$0.31 \times 0.17 \times 0.11$
Crystal class	hexagonal
Space group	$P3_1/c$
a (Å)	12.6614(7)
b (Å)	–
c (Å)	10.9299(5)
α (°)	–
β (°)	–
γ (°)	–
V (Å^3)	1517.44(14)
Z	2
μ (Mo Kα) (mm^{-1})	0.589
T (K)	300(2)
Radiation, λ (Å)	0.71073
Measured reflections	6659
Independent reflections	2124
R_{int}	0.046
Absorption correction	Multi-scan
Min/max transmission	0.84, 0.94
Observed reflections [$I > 2\sigma(I)$]	1834
Range in 2θ (°)	$6.4 \leqslant 2\theta \leqslant 54.9$
Range in h	$-14 \leqslant h \leqslant 16$
Range in k	$-16 \leqslant k \leqslant 15$
Range in l	$-14 \leqslant l \leqslant 14$
Parameters/restraints	175/1
$R(F)$ [a], $wR(F^2)$ [b]	0.043, 0.108

Table 1 (*Continued*)

	$[Fe(L^1)_3](BF_4)_2\cdot 2H_2O$ ($\mathbf{3}\cdot 2H_2O$)
Goodness of fit	1.049
Weighting scheme [c]	$w = 1/[\sigma^2(F_o^2)+(0.0491P)^2 +0.5213P]$
$\Delta\rho$ (max/min) (e Å^{-3})	0.22/−0.23
Flack parameter	−0.01(3)

[a] $R = \Sigma[|F_o|-|F_c|]/\Sigma|F_o|$.
[b] $wR = [\Sigma w(F_o^2-F_c^2)/\Sigma wF_o^4]^{1/2}$.
[c] $P = (F_o^2+2F_c^2)/3$.

2.6. X-ray structure determination of $[Fe(L^1)_3](ClO_4)_2\cdot H_2O$ ($\mathbf{2}\cdot H_2O$)

The solvent water molecule is disordered over three sites, with occupancies of 0.60:0.20:0.20. One ClO_4^- anion is disordered over two orientations, with an occupancy ratio 0.60:0.40. All Cl–O distances in the disordered anion were restrained to 1.43(2) Å, and non-bonded O···O distances within a given disorder orientation to 2.34(2) Å. Finally, one pyrazole group C(19)–C(23) is disordered, over two orientations with occupancies of 0.75 and 0.25. This was modeled using the restraints N–N = 1.36(2), N–C = 1.35(2), N=C = 1.32(2), C–C{intra-ring} = 1.39(2), C–C{inter-ring} = 1.45(2) and C=C = 1.36(2) Å. All non-H atoms with occupancy >0.5 were refined anisotropically. The H atoms for the disordered water molecule could not be located in the difference map, and so were not included in the final refinement. All other H atoms were placed in calculated positions and refined using a riding model.

2.7. X-ray structure determination of $[Fe(L^1)_3](BF_4)_2\cdot 2H_2O$ ($\mathbf{3}\cdot 2H_2O$)

The asymmetric unit contains one-third of a complex dication, with Fe(1) lying on the crystallographic C_3 axis 2/3, 1/3, z, and one-third of a BF_4^- anion with one B–F bond lying on the axis 1/3, 2/3, z. There is also a very badly disordered region in the difference map, corresponding to the interior of the channels in the crystal, which was modeled using 9 (150 K) or 12 (300 K) partial O environments to a total of two O atoms per asymmetric unit. From the microanalysis of the crystals and NMR data, this disordered region is presumed to contain the second BF_4^- anion, which was otherwise not located in the difference map, as well as some water. At 300 K only, the resolved BF_4^- ion was disordered by rotation about its C_3 axis. Three partial F environments were modeled for the disordered F atom F(15), with occupancies of 0.40, 0.35 and 0.25, using the restraints B–F = 1.38(1) Å and F···F = 2.25(2) Å. At both temperatures, all wholly occupied non-H atoms were refined anisotropically. The pyrrolic H atom H(10) was located in the difference map and allowed to refine freely, while all C-bound H atoms were placed in calculated positions and refined using a riding model. No H atoms attached to the disordered partial O atoms could be detected in the difference map, and these were not included in the final model.

2.8. Other measurements

Infra-red spectra were obtained as Nujol mulls pressed between KBr windows, between 400 and 4000 cm^{-1} using a Nicolet Avatar 360 spectrophotometers. UV/visible spectra were obtained with a Perkin–Elmer Lambda 900 spectrophotometer, operating between 1100 and 200 nm, in 1 cm quartz cells. Positive ion FAB mass spectra were performed on a VG AutoSpec spectrometer, employing a 3-NOBA matrix. CHN microanalyses were performed by the University of Leeds School of Chemistry microanalytical service. Solution ^{1}H NMR spectra were run on a Bruker ARX250 spectrometer, operating at 250.1 MHz. Solid state NMR spectra were obtained using a Bruker MSL300 instrument, operating at 281.8 (^{19}F) and 96.1 (^{11}B) MHz, and were referenced to $BF_3\cdot Et_2O$.

3. Results and discussion

Reaction of hydrated $FeCl_2$ with three molar equivalents of L^1 in water gave a maroon solution, which yielded a sparingly soluble maroon powder on slow evaporation. Recrystallisation of this solid from MeOH/Et_2O gave $[FeCl_2(L^1)_2]\cdot H_2O$ ($\mathbf{1}\cdot H_2O$) as the only isolable pure product. We have been unable to prepare $[Fe(L^1)_3]Cl_2$ in pure form by this, or any other, route. In contrast, $[Fe(L^1)_3](ClO_4)_2\cdot H_2O$ ($\mathbf{2}\cdot H_2O$) and $[Fe(L^1)_3](BF_4)_2\cdot 2H_2O$ ($\mathbf{3}\cdot 2H_2O$) were obtained cleanly from analogous aqueous complexations of hydrated $Fe(ClO_4)_2$ and $Fe(BF_4)_2$. Although clearly showing the presence of two BF_4^- anions, the F analysis of different samples of $\mathbf{3}\cdot 2H_2O$ was variable and consistently low by 0.8–1.5%, which may reflect partial hydrolysis of the BF_4^- ions during the aqueous complexation (see below) [17]. The presence of water in $\mathbf{1}\cdot H_2O$, $\mathbf{2}\cdot H_2O$ and $\mathbf{3}\cdot 2H_2O$ was confirmed by IR spectroscopy, which showed

a characteristic H–O–H bending vibration as a broad peak near 1630 cm^{-1} [18].

The ^1H NMR spectrum of **3**·$2H_2O$ in CD_3CN is broadened, and shows two major L^1 environments (Section 2). First are six peaks between δ 10.2 and 17.0 ppm with approximately equal integrals. We assign this species to a Fe-containing species that is in a spin-state equilibrium, with only a small high-spin fraction at 300 K (because of its small contact shifts). Second, are five peaks of equal integral in the range 6.9–9.2 ppm, whose chemical shifts are identical to those of uncoordinated L^1 in this solvent. Spectra obtained in $\{CD_3\}_2CO$ or CD_3NO_2 show similar peaks, but with the relative abundance of the two L^1 environments varying between the solvents. These data strongly suggest that partial solvolysis of the Fe centres occurs upon dissolution. Consistent with this, the FAB mass spectra of **2** and **3** contain no molecular ions derived from $[Fe(L^1)_3]^+$. Rather, peaks from ions with a 2:1 L^1:Fe stoichiometry are dominant, which also shows that the L^1 ligands are labile under these conditions. Unfortunately, **1**·H_2O was insufficiently soluble for its NMR spectrum to be obtained.

The single crystal structure of **1**·H_2O shows a six-coordinate Fe(II) centre with approximate C_2 symmetry, with *cis*-Cl^- ligands and *trans*-L^1 pyridine donors (Fig. 1, Table 2). The bond lengths to Fe are consistent with a high-spin Fe(II) centre, as is usual for Fe(II) complexes with a dichloro-tetraaza donor set [19,20]. Interestingly, the C_2 symmetry at Fe(1) is broken by the two Fe–Cl bond lengths, the bond Fe(1)–Cl(24) being 0.0644(8) Å longer than Fe(1)–Cl(25). This distortion is also reflected in the angles N(2)–Fe(1)–Cl(24) and N(13)–Fe(1)–Cl(25), which differ by 3.56(7)°; and, N(2)–Fe(1)–N(20) and N(9)–Fe(1)–N(13), which differ by 2.64(10)°. All other bonds and angles related by the pseudo-C_2 axis differ by much smaller amounts, or are crystallographically equal. This type of distortion involving unequal Fe–Cl distances has only been observed once before in a $Fe^{II}Cl_2N_4$ complex [20]. Since Cl(24) and Cl(25) accept near-identical O–H···Cl hydrogen bonds (see below), it is unclear why **1** should exhibit this structural distortion.

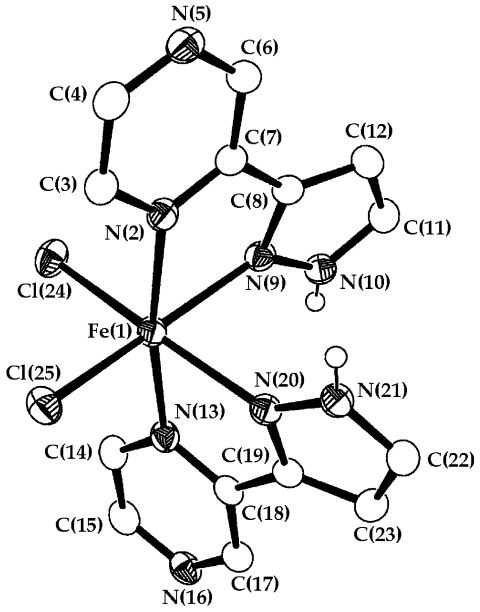

Fig. 1. View of the complex molecule in the single crystal structure of $[FeCl_2(L^1)_2]\cdot H_2O$ (**1**·H_2O), showing the atom numbering scheme employed. All C-bound H atoms have been omitted for clarity. Thermal ellipsoids are at the 50% probability level.

Table 2
Selected bond lengths (Å) and angles (°) in the single crystal X-ray structures of $[FeCl_2(L^1)_2]\cdot H_2O$ (**1**·H_2O).

Bond lengths	
Fe(1)–N(2)	2.1896(18)
Fe(1)–N(9)	2.2290(19)
Fe(1)–N(13)	2.1995(18)
Fe(1)–N(20)	2.2207(19)
Fe(1)–Cl(24)	2.4510(6)
Fe(1)–Cl(25)	2.3866(6)
Bond angles	
N(2)–Fe(1)–N(9)	74.25(7)
N(2)–Fe(1)–N(13)	170.16(7)
N(2)–Fe(1)–N(20)	99.47(7)
N(2)–Fe(1)–Cl(24)	90.95(5)
N(2)–Fe(1)–Cl(25)	93.56(5)
N(9)–Fe(1)–N(13)	96.83(7)
N(9)–Fe(1)–N(20)	78.73(7)
N(9)–Fe(1)–Cl(24)	92.72(5)
N(9)–Fe(1)–Cl(25)	164.64(5)
N(13)–Fe(1)–N(20)	74.29(7)
N(13)–Fe(1)–Cl(24)	93.66(5)
N(13)–Fe(1)–Cl(25)	94.51(5)
N(20)–Fe(1)–Cl(24)	164.07(5)
N(20)–Fe(1)–Cl(25)	94.49(5)
Cl(24)–Fe(1)–Cl(25)	96.87(2)

The lattice water molecule in **1**·H_2O forms hydrogen bonds to Cl(25), and to Cl(24′) of a neighbouring molecule related by $x+1$, y, z. The two pyrazole N–H groups of the complex also form the following hydrogen bonds to pyrazine N-atoms: N(10)–H(10)···N(16″) (related by $-x+2$, $-y+1$, $-z+2$); and N(21)–H(21)···N(5‴) (related by $-x+1$, $-y+1$, $-z+1$). This results in a 2D lattice, with co-parallel chains of hydrogen-bonded complex molecules spanned by water molecules (Fig. 2). Adjacent complex molecules within the chains are also linked by π–π interactions between their pyrazine rings N(2)–C(7) and N(2‴)–C(7‴), which are separated by 3.225(12) Å and offset by 1.48 Å; and, N(13)–C(18) and N(13″)–C(18″), separated by 3.26(2) Å and offset by 1.35 Å.

The complex dication in **2**·H_2O has a distorted *mer*-octahedral structure that resembles that in $[Fe(L^2)_3](O_3SCF_3)_2\cdot 2H_2O$ [11], $[Fe(L^3H)_3](BF_4)_2\cdot 2H_2O$ [13] and $[Fe(L^3Me)_3](BF_4)_2$ [12] (Fig. 3, Table 3). The Fe–N bond lengths in **2** are consistent with the Fe

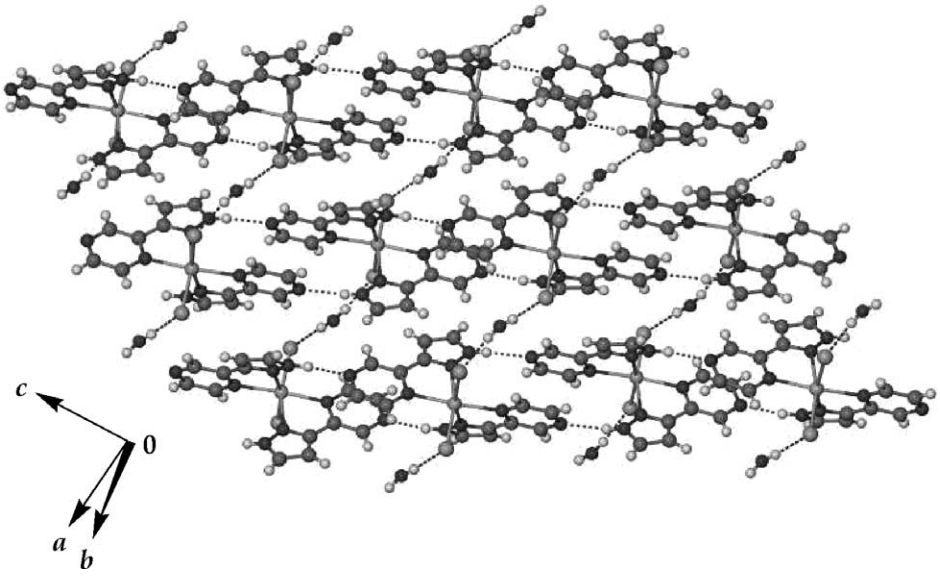

Fig. 2. Packing diagram of $\mathbf{1}\cdot H_2O$.

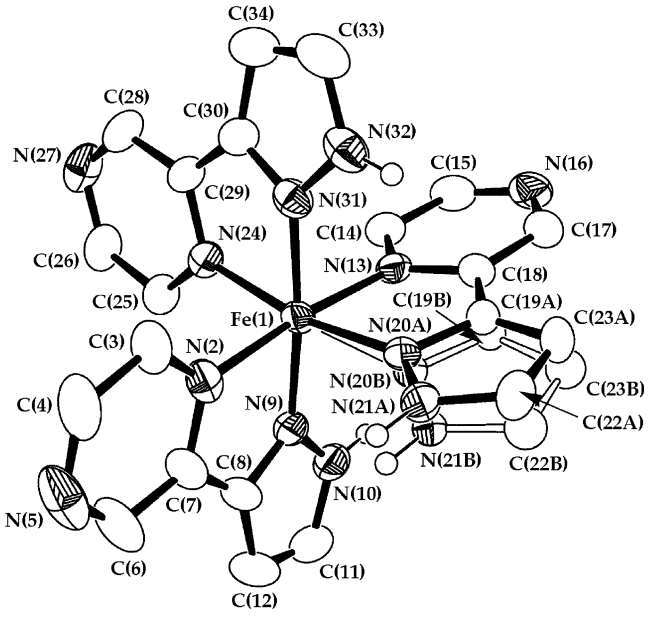

Fig. 3. View of the complex dication in the single crystal structure of $[Fe(L^1)_3](ClO_4)_2\cdot H_2O$ ($\mathbf{2}\cdot H_2O$). All C-bound H atoms have been omitted for clarity. Thermal ellipsoids are at the 50% probability level. Both the major (solid bonds) and minor (hollow bonds) disorder orientations of the disordered pyrazole group C(19)–C(23) are shown.

content of the crystal being purely low-spin at the temperature of the experiment (150 K). The pyrazole ring of one of the ligands is disordered over a major (75%) and minor (25%) orientation (Fig. 3). This disorder is linked to disorder in the solvate water molecule (Section 2), since one 20%-occupied partial O environment lies within van der Waals contact of the major ligand orientation. This suggests that the major ligand orientation, and this partial water site, cannot be simultaneously occupied. There is a complex pattern of

Table 3
Selected bond lengths (Å) and angles (°) in the single crystal X-ray structures of $[Fe(L^1)_3](ClO_4)_2\cdot H_2O$ ($\mathbf{2}\cdot H_2O$)

Bond lenghts	
Fe(1)–N(2)	1.979(3)
Fe(1)–N(9)	1.946(3)
Fe(1)–N(13)	1.983(3)
Fe(1)–[N(20A), N(20B)]	1.936(6), 2.01(2)
Fe(1)–N(24)	1.969(3)
Fe(1)–N(31)	1.954(3)
Bond angles	
N(2)–Fe(1)–N(9)	80.27(13)
N(2)–Fe(1)–N(13)	173.95(12)
N(2)–Fe(1)–[N(20A), N(20B)]	94.20(19), 96.8(6)
N(2)–Fe(1)–N(24)	91.14(11)
N(2)–Fe(1)–N(31)	96.40(13)
N(9)–Fe(1)–N(13)	96.31(12)
N(9)–Fe(1)–[N(20A), N(20B)]	94.9(2), 85.8(6)
N(9)–Fe(1)–N(24)	95.61(12)
N(9)–Fe(1)–N(31)	174.51(13)
N(13)–Fe(1)–[N(20A), N(20B)]	81.1(2), 77.9(6)
N(13)–Fe(1)–N(24)	94.17(11)
N(13)–Fe(1)–N(31)	87.39(12)
[N(20A), N(20B)]–Fe(1)–N(24)	168.9(2), 172.1(6)
[N(20A), N(20B)]–Fe(1)–N(31)	89.7(2), 99.0(6)
N(24)–Fe(1)–N(31)	80.03(13)

The two values quoted for bonds and angles to N(20) correspond respectively to the two disorder orientations of this atom, N(20A) and N(20B).

intermolecular N–H···N, N–H···O and O–H···O hydrogen bonding in the lattice, leading to a 3D network of hydrogen-bonded molecules.

In contrast to **2**, the complex dication in $\mathbf{3}\cdot 2H_2O$ has crystallographic C_3 symmetry and adopts a *fac*-octahedral stereochemistry that is distorted by the small ligand bite-angle (Table 4, Fig. 4). As for **2**, the Fe ion in **3** is clearly low-spin at 150 K, from the Fe–N bond lengths

Table 4
Selected bond lengths (Å) and angles (°) in the single crystal X-ray structures of $[Fe(L^1)_3](BF_4)_2\cdot 2H_2O$ ($3\cdot 2H_2O$)

	150 K	300 K
Bond lengths		
Fe(1)–N(2)	1.9767(19)	1.981(3)
Fe(1)–N(9)	1.962(2)	1.960(3)
Bond angles		
N(2)–Fe(1)–N(2′)	94.56(8)	94.72(12)
N(2)–Fe(1)–N(9)	80.39(9)	80.18(12)
N(2)–Fe(1)–N(9′)	89.71(9)	88.85(13)
N(2′)–Fe(1)–N(9)	173.65(10)	174.01(14)
N(9)–Fe(1)–N(9′)	95.65(8)	96.50(12)

Primed atoms are related to unprimed atoms by the relation $1-y$, $x-y$, z.

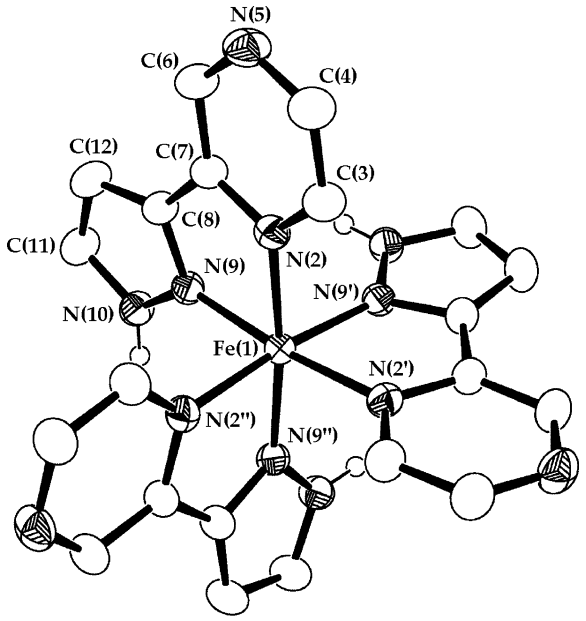

Fig. 4. View of the complex dication in the single crystal structure of $[Fe(L^1)_3](BF_4)_2\cdot 2H_2O$ ($3\cdot 2H_2O$). All C-bound H atoms have been omitted for clarity. Thermal ellipsoids are at the 50% probability level. Primed atoms are related to unprimed atoms by the relation $-y+1$, $x-y$, z; and, doubly primed atoms by $x+y-1$, $-x+1$, z.

in the structure. The pyrazole N–H group hydrogen bonds to the pyrazine atom N(5′) of a neighbouring molecule related by $x-y+1$, $-y+1$, $z+1/2$. The effect of this is to associate the complex molecules into a hexagonal honeycomb, with channels running parallel to the crystallographic c axis (Fig. 5). Only one BF_4^- anion was located in the Fourier map, which has crystallographic C_3 symmetry and occupies a cavity within the 'walls' of the honeycomb. The channels are filled with a highly disordered region of electron density that could not be positively identified, but presumably contains the other BF_4^- ion and water that are present by microanalysis. The 'missing' content of the crystals as calculated by microanalysis, of $1/3BF_4^- + 2/3H_2O$ per crystallographic asymmetric unit, are consistent with the amount of intra-pore disordered electron density, which is approximately equivalent to two O atoms per asymmetric unit.

In order to determine whether $3\cdot 2H_2O$ undergoes a spin-state transition upon cooling (which would lead to a change in the crystal pore sizes), a second X-ray analysis at 300 K was performed on the same crystal of this compound that was used for the low temperature analysis. The crystal is isomorphous at the two temperatures, and the metric parameters at Fe are indistinguishable at 150 and 300 K. Therefore, $3\cdot 2H_2O$ contains purely low-spin Fe centres at both temperatures. However, the intra-pore disorder is more complex at 300 K than at 150 K, which could mean that the contents of the pores are dynamically disordered at either or both of these temperatures, and/or that the arrangement of molecules within the pores is different at 300 K than at 150 K. We suggest that this ordering and/or rearrangement of the pore contents upon cooling is responsible for a small *increase* in the unit cell volume of $3\cdot 2H_2O$ at 150 K compared to 300 K (Table 1). This reflects the unit cell parameter c, which runs parallel to the pores (Fig. 5), being 0.0529(5) Å longer at 150 K.

The closest interatomic distance spanning the channels through the crystal of $3\cdot 2H_2O$ is $H(11)\cdots H(4'') = 7.7$ Å at 150 K (related by $y+1$, $x+1$, $z+1/2$), corresponding to a pore diameter of 5.3 Å given that the van der Waals radius of hydrogen is 1.2 Å [22]. Since the effective diameter of BF_4^- is 4.2 Å [23] and that of H_2O is approximately 2.6 Å [24], the formulation of the solid suggests that the channels in $3\cdot 2H_2O$ are tightly packed with BF_4^- and water, so that mobility of these molecules through the pores could be restricted. Consistent with this, the microanalysis of $3\cdot 2H_2O$ is unchanged following heating to 100 °C under vacuum for 48 h, showing that the water content of the pores is not easily lost. Soaking $3\cdot 2H_2O$ in a solution of toluene saturated with NBu^n_4Cl for 48 h yielded a sample with a Cl analysis of $2.1\pm 0.1\%$, which is equivalent to the replacement of approximately 0.4 mol equivalents of BF_4^- by Cl^-. However, this is accompanied by partial visual decomposition of the crystals, showing that the structural integrity of $3\cdot 2H_2O$ is not retained during this procedure. We found no other solvent, in which NBu^n_4Cl is soluble but $3\cdot 2H_2O$ is apparently insoluble, that could be used as an alternative medium for this anion replacement.

In order to further probe the anion content of $3\cdot 2H_2O$, solid state ^{19}F and ^{11}B NMR spectra were obtained from this compound at 293 K. The ^{19}F spectra showed two singlets with similar integrals, at δ −142.4 and −146.2 ppm. There is also a weak shoulder at −144.0 ppm, which we tentatively attribute to a fraction of BF_3OH^- ions in the sample (see above), since the ^{19}F chemical shifts of BF_4^- and BF_3OH^- are very similar

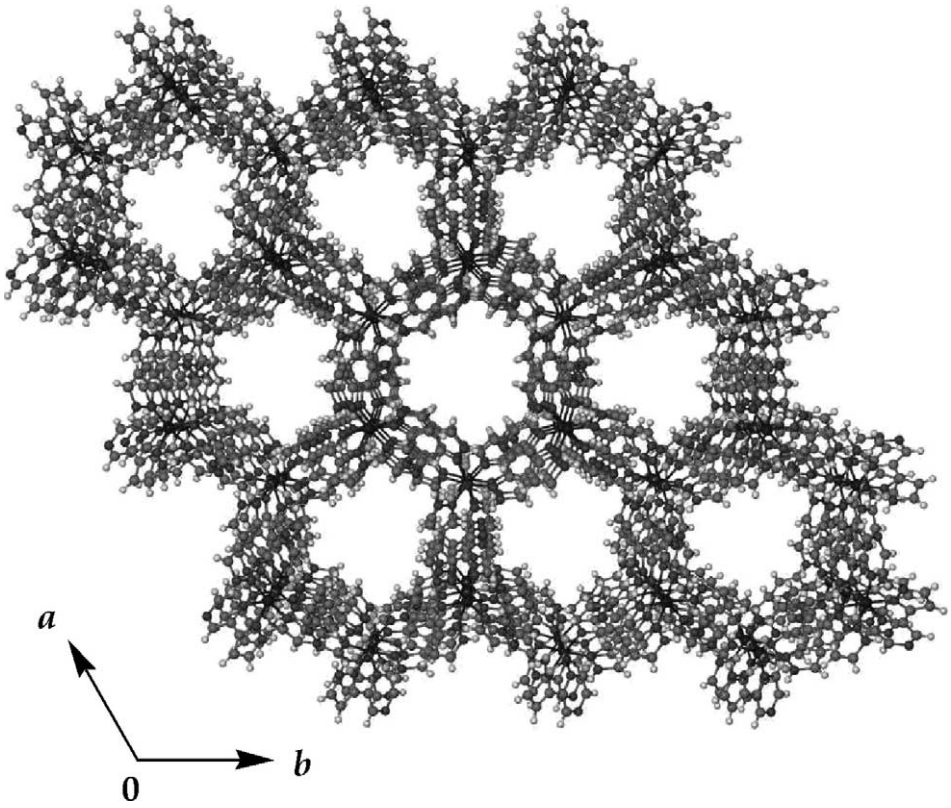

Fig. 5. Packing diagram of $\mathbf{3}\cdot 2H_2O$, viewed perpendicular to the *ab* plane. The well-defined BF_4^- anions are shown, but the disordered contents of the pores, and all hydrogen bonds within the structure, have been omitted for clarity.

[25]. Similar results were obtained from ^{11}B NMR, for which two singlets of approximately equal integral were obtained, at δ 1.2 and 3.6 ppm. The ^{19}F and ^{11}B line widths were both narrow, consistent with both BF_4^- environments in the solid rotating rapidly at this temperature. Following heating of crystalline $\mathbf{3}\cdot 2H_2O$ at 100 °C under vacuum for 48 h, the ^{19}F and ^{11}B NMR spectra of the ground sample were broadened, but otherwise unchanged. We suggest that this may reflect some loss of crystallinity during the annealing process.

4. Concluding remarks

Compound $\mathbf{3}\cdot 2H_2O$ is an unusual example of a porous structure constructed from a 3D hydrogen-bonded network, rather than from a coordination polymer [14,26]. In principle, the weaker intermolecular interactions within the walls of the structure might be expected to lead to a poorly robust material. We therefore attribute the inertness of $\mathbf{3}\cdot 2H_2O$ to water loss to a combination of the small size of the pores in this crystal, which are only slightly bigger than the intra-pore BF_4^- ions; and, the strong electrostatic interactions that hold these anions in place. This is likely to sterically block movement, and loss, of the water content of the channels. The honeycomb structure in $\mathbf{3}\cdot 2H_2O$ is also chiral, being in the space group $P3_1/c$. The chirality arises from the octahedral *fac*-$[Fe(L^1)_3]^{2+}$ centres, which can have Λ or Δ configurations [21]; in the crystal analysed, all the Fe centres are in the Λ form. As a result, the C_3-symmetric, three-connected hydrogen bonding topology that links the complex dications is also chiral.

It is a little surprising that $[Fe(L^1)_3]^{2+}$ appears to favour a low-spin configuration, given that all reported salts of $[Fe(L^2)_3]^{2+}$ and $[Fe(L^3R)_3]^{2+}$ (R = H, Me) are spin-crossover compounds at room temperature or below [10–13]. The pyrazine donor in L^1 will be less basic than the pyridine donor in L^2 by several *p*K units [27], which might be expected to favour a high-spin-state for $[Fe(L^1)_3]^{2+}$, contrary to our observations. The low-spin configuration may be enforced on $\mathbf{3}\cdot 2H_2O$ by the steric constraints of the surrounding hydrogen-bonded lattice [1], and it is possible that $\mathbf{2}\cdot H_2O$ (at $T > 150$ K) and other salts of $[Fe(L^1)_3]^{2+}$ might have the desired, spin-crossover character. We are currently investigating that possibility.

5. Supplementary data

Full crystallographic data for the structure analyses in this study are available on request from the Cambridge

Crystallographic Data Centre, 12 Union Road, Cambridge, CB2 1EZ, UK (fax: +44-1223-336033; e-mail: deposit@ccdc.cam.ac.uk or http://www.ccdc.cam.ac.uk. The CCDC deposition numbers are 186162 (**1**·H_2O), 186161 (**2**·H_2O), 186160 (**3**·$2H_2O$ at 150 K) and 186159 (**3**·$2H_2O$ at 300 K).

Acknowledgements

The authors thank the Royal Society for a research fellowship to M.A.H., and the University of Leeds for funding.

References

[1] P. Gütlich, A. Hauser, H. Spiering, Angew. Chem., Int. Ed. 33 (1994) 2024.
[2] P. Gütlich, Y. Garcia, H.A. Goodwin, Chem. Soc. Rev. 29 (2000) 419.
[3] O. Kahn, Science 179 (1998) 44.
[4] (a) J. Kröber, E. Codjovi, O. Kahn, F. Grolière, C. Jay, J. Am. Chem. Soc. 115 (1993) 9810;
(b) J. Kröber, J.-P. Audière, E. Codjovi, O. Kahn, J.G. Haasnoot, F. Grolière, C. Jay, A. Bousseksou, J. Linarès, F. Varret, A. Gonthier-Vassal, Chem. Mater. 6 (1994) 1404;
(c) Y. Garcia, P.J. van Koningsbruggen, R. Lapouyade, L. Fournès, L. Rabardel, O. Kahn, V. Ksenofontov, G. Levchenko, P. Gütlich, Chem. Mater. 10 (1998) 2426;
(d) O. Roubeau, J.M. Alcazar Gomez, E. Balskus, J.J.A. Kolnaar, J.G. Haasnoot, J. Reedijk, New J. Chem. 25 (2001) 144.
[5] (a) W. Fujita, K. Agawa, Science 286 (1999) 261;
(b) G.D. McManus, J.M. Rawson, N. Feeder, J. van Duijn, E.J.L. McInnes, J.J. Novoa, R. Burriel, F. Palacio, P. Oliete, J. Mater. Chem. 11 (2001) 1992.
[6] J.M. Holland, J.A. McAllister, Z. Lu, C.A. Kilner, M. Thornton-Pett, M.A. Halcrow, Chem. Commun. (2001) 577.
[7] J.M. Holland, J.A. McAllister, C.A. Kilner, M. Thornton-Pett, A.J. Bridgeman, M.A. Halcrow, J. Chem. Soc., Dalton Trans. (2002) 548.
[8] J.M. Holland, C.A. Kilner, M.A. Halcrow, Inorg. Chem. Commun. 5 (2002) 328.
[9] K.L.V. Mann, J.C. Jeffrey, J.A. McCleverty, M.D. Ward, Polyhedron 18 (1999) 721.
[10] K.H. Sugiyarto, H.A. Goodwin, Aust. J. Chem. 41 (1988) 1645.
[11] L.S. Harimanow, K.H. Sugiyarto, D.C. Craig, M.L. Scudder, H.A. Goodwin, Aust. J. Chem. 52 (1999) 109.
[12] K.H. Sugiyarto, D.C. Craig, A.D. Rae, H.A. Goodwin, Aust. J. Chem. 48 (1995) 35.
[13] A.F. Stassen, M. de Vos, P.J. van Koningsbruggen, F. Renz, J. Ensling, H. Kooijman, A.L. Spek, J.G. Haasnoot, P. Gütlich, J. Reedijk, Eur. J. Inorg. Chem. (2000) 2231.
[14] See e.g. (a) S.S.Y. Chui, S.M.-F. Lo, J.P.H. Charmant, A.G. Orpen, I.D. Williams, Science 283 (1999) 1148;
(b) T.M. Reineke, M. Eddadoui, M. Fehr, D. Kelley, O.M. Yaghi, J. Am. Chem. Soc. 121 (1999) 1651;
(c) B. Chen, M. Eddadoui, S.T. Hyde, M. O'Keefe, O.M. Yaghi, Science 291 (2000) 1021;
(d) S. Noro, S. Kitagawa, M. Kondo, K. Seki, Angew. Chem., Int. Ed. 39 (2000) 2081; < sp = 1 > (e) A.J. Blake, N.R. Champness, A.N. Khlobystov, S. Parsons, M. Schröder, Angew. Chem., Int. Ed. 39 (2000) 2317;
(f) K. Biradha, Y. Hongo, M. Fujita, Angew. Chem., Int. Ed. 39 (2000) 3843;
(g) T.M. Reineke, M. Eddadoui, D. Moler, M. O'Keefe, O.M. Yaghi J. Am. Chem. Soc. 122 (2000) 4843;
(h) L. Pan, E.B. Woodlock, X. Wang, C. Zheng, Inorg. Chem. 39 (2000) 4174;
(i) X. Xu, M. Nieuwenhuyzen, S.L. James, Angew. Chem., Int. Ed. 41 (2002) 764.
[15] G.M. Sheldrick, Acta Crystallogr., Sect. A 46 (1990) 467.
[16] G.M. Sheldrick, SHELXL-97, Program for the Refinement of Crystal Structures, University of Göttingen, 1997.
[17] For examples of the serendipitous aqueous hydrolysis of BF_4^- — see e.g. (a) J. Telser, R.S. Drago, Inorg. Chem. 23 (1984) 1798;
(b) R.C. Kerber, K.P. Reis, J. Org. Chem. 54 (1989) 3550;
(c) D. Onggo, D.C. Craig, A.D. Rae, H.A. Goodwin, Aust. J. Chem. 44 (1991) 219;
(d) S.G. Bott, A. Alvanipour, J.L. Atwood, J. Inclusion Phenom. Mol. Recog. Chem. 10 (1991) 153;
(e) H. Feinberg, I. Columbus, S. Cohen, M. Rabinovitz, H. Selig, G. Shoham, Polyhedron 12 (1993) 2913;
(f) M. Ghiladi, K.B. Jensen, J. Jaing, C.J. McKenzie, S. Morup, I. Sotofte, J. Ulstrup, J. Chem. Soc., Dalton Trans. (1999) 2675.
[18] K. Nakamoto, in: K. Nakamoto (Ed.), Infrared and Raman Spectra of Inorganic and Coordination Compounds, Part B, Wiley Interscience, New York, 1997, p. 54.
[19] (a) G.J. Long, P.J. Clark, Inorg. Chem. 17 (1978) 1394;
(b) S.C. Davies, D.L. Hughes, G.J. Leigh, J.R. Sanders, J.S. de Souza, J. Chem. Soc., Dalton Trans. (1997) 1981;
(c) P. Karsten, J. Strähle, Acta Crystallogr., Sect. C 54 (1998) 1406;
(d) J.-S. Sun, H. Zhao, X. Ouyang, R. Clérac, J.A. Smith, J.M. Clemente-Juan, C. Gómez-Garcia, E. Coronado, K.J. Dunbar, Inorg. Chem. 38 (1999) 5841;
(e) T.J. Hubin, J.M. McCormick, S.R. Collinson, M. Buchalova, C.M. Perkins, N.W. Alcock, P.K. Kahol, A. Rughanuthan, D.H. Busch, J. Am. Chem. Soc. 122 (2000) 2512;
(f) J. Simaan, S. Poussereau, G. Blondin, J.-J. Girerd, D. Defaye, C. Philouze, J. Guilhem, L. Tchertanov, Inorg. Chim. Acta 299 (2000) 221;
(g) Y. Mekmouche, S. Ménage, C. Toia-Duboc, M. Fontecave, J.-B. Galey, C. Lebrun, J. Pécaut, Angew. Chem., Int. Ed. 40 (2001) 949.
[20] B. Rieger, A.S. Abu-Surrah, R. Fawzi, M. Steiman, J. Organomet. Chem. 497 (1995) 73.
[21] A. von Zelewsky, Stereochemistry of Coordination Compounds, Wiley, Chichester, 1996, pp. 101–106.
[22] L. Pauling (Ed.), The Nature of the Chemical Bond, third ed., Cornell University Press, Ithaca, NY, 1960, pp. 257–264.
[23] D.M.P. Mingos, A.L. Rohl, J. Chem. Soc., Dalton Trans. (1991) 3419.
[24] M. Gerstein, J. Tsai, M. Levitt, J. Mol. Biol. 249 (1995) 955.
[25] (a) R.E. Mesmer, A.C. Rutenberg, Inorg. Chem. 12 (1973) 699;
(b) J.W. Akitt, J. Chem. Soc., Faraday Trans. 71 (1975) 1557.
[26] B. Moulton, M.J. Zaworotko, Chem. Rev. 101 (2001) 1629.
[27] A. Albert, R. Goldacre, J. Phillips, J. Chem. Soc. (1948) 2240.